

## A GIS methodology for the analysis of weather radar precipitation data

M. A. Gad and I. K. Tsanis

### ABSTRACT

A GIS multi-component module was developed within the ArcView GIS environment for processing and analysing weather radar precipitation data. The module is capable of: (a) reading geo-reference radar data and comparing it with rain-gauge network data, (b) estimating the kinematics of rainfall patterns, such as the storm speed and direction, and (c) accumulating radar-derived rainfall depths. By bringing the spatial capabilities of GIS to bear this module can accurately locate rainfall on the ground and can overlay the animated storm on different geographical features of the study area, making the exploration of the storm's kinematic characteristics obtained from radar data relatively simple. A case study in the City of Hamilton in Ontario, Canada is used to demonstrate the functionality of the module. Radar comparison with rain gauge data revealed an underestimation of the classical Marshal & Palmer Z-R relation to rainfall rate.

**Key words** | GIS, precipitation, radar, storm kinetics

M. A. Gad  
I. K. Tsanis (corresponding author)  
Department of Civil Engineering,  
1280 Main Street West,  
Hamilton,  
Ontario,  
Canada L8S 4L7

### INTRODUCTION

The use of Geographical Information Systems (GIS) was originally limited to the geographical field in different applications, such as the set-up of multi-dimension information, analysis, utility and display. Nowadays, it has reached far beyond the limited concept of graphics and provides support for many applications. For example, GIS can provide powerful tools for storing, managing, analysing, displaying and modelling different spatiotemporal environmental processes.

ArcView GIS is a PC-based software program that offers a user-friendly interface and powerful functions for spatial operations. One of its extensions, the spatial analyst extension, implements a large number of member functions (analysis requests) within the Grid class. These member functions provide different operations for the analysis of raster data. Examples of these operations are the local statistical operations, focal and zonal statistical operations, geometric and distance operations, and other global merging operations.

In addition to these built-in capabilities, ArcView GIS maintains a powerful feature which is the ability to

establish conversations with externally and dynamically linked libraries (DLLs). The main advantage of such DLLs is that they can extend the functionality of an application without recompiling the original executable because the external modules in this case are dynamically linked to the application at run time. ArcView provides classes and requests that support the loading and calling of procedures in these types of libraries. The advantages described above makes ArcView GIS one of the favourable platforms for studying different point, areal and, especially, continuous processes.

Rainfall patterns are examples of such continuous processes that can be analysed in a GIS environment. Rainfall fields contain a complicated mixture of cloud structures which are developing and dissipating, come close to each other or go apart and, in doing so, move across the catchment (Austin & Houze 1972; Amorocho & Wu 1977; Gupta & Waymyre 1979; and others). Radar scans can provide different information concerning rainfall characteristics (Huff *et al.* 1981; Collier 1989; and others). The contribution of weather radar to the

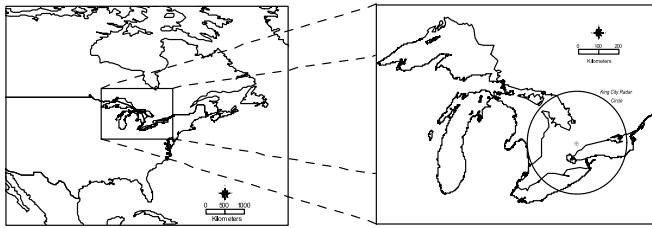


Figure 1 | Location of the study area.

description of the behaviour of precipitation, a major part of the hydrological cycle, has been of considerable interest over many years. The radar data is important to the fields of meteorology and hydrology in measuring and forecasting precipitation as well as their corresponding uses in watershed modelling and flood forecasting. For those research scientists and engineers who have the opportunity to use radar rainfall data, the managing and processing of large amounts of radar data is problematic. A further problem relates to the understanding of aspects of the rainfall process as revealed by radar scans. Hence, the aim of this study is to provide a flexible and suitable platform for handling radar rainfall data. This platform is the ArcView GIS.

In the following sections, a summary of the radar measurements of precipitation is presented, the format of the CAPPI data (Constant Altitude Plane Position Indicator) is described, and the description of the theories and technical details of the different components of the module is explained. The case study used to illustrate the functionality of the module is the City of Hamilton. The radar data was obtained from the King City radar site, Ontario, Canada (see Figure 1). A few storm events were analysed and the results are presented.

## DESCRIPTION OF CAPPI RADAR DATA

More details of radar observations of weather phenomena can be found in different references, such as Skolnik (1970) for engineering and equipment aspects, Sauvageot (1982), Battan (1981) and Collier (1989) for meteorological phenomena and applications, Atlas (1964, 1990) for

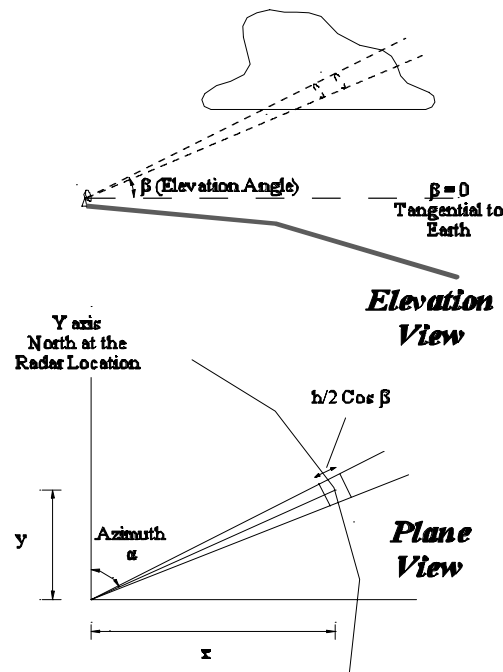


Figure 2 | The radar measurement of precipitation (note the radar coordinate system).

general reviews, Rinehart (1991) for modern techniques, and Doviak & Zrnica (1993) for Doppler radar principles and applications (Joe 1999). A summary of the basic theory of radar measurements of precipitation and the format of the radar rainfall product are presented below.

## Radar observations of precipitation

Most meteorological radars are pulsed radars, that is, electromagnetic waves at fixed preferred frequencies are transmitted from a directional antenna into the atmosphere in a rapid succession or train of microwave pulses. Figure 2 shows a directional radar antenna emitting a pulsed beam of electromagnetic energy and illuminating a portion of a meteorological target (Joe 1999). The train of electromagnetic pulses is absorbed and scattered by any meteorological targets encountered. Between successive pulses, the receiver listens for any return of the wave. The returned signal from the target is commonly referred to as the radar echo. The strength of the signal reflected back to the radar receiver from the target is a function of the

concentration, size and water phase of the precipitation particles comprising the target. The radar range equation relates the power return from the target to the radar characteristics and parameters of the target. One of the most important meteorological parameters of the target is the reflectivity factor  $Z$ , which can be converted later to rainfall rate  $R$  using a  $Z$ - $R$  relation.

The power measurements are determined by the total power back-scattered by the target within a volume being sampled at any one instant (the pulse volume). The returned power may be integrated later in both space and time. The pulse volume dimensions are dependent on the radar pulse length  $h$  in space and the antenna beam widths in the vertical and the horizontal (usually  $0.5$ – $1^\circ$ ). Since the power which arrives back at the radar at the same instant of time is involved in a two-way path, the pulse-volume-length is only one-half the pulse length in space ( $h/2$ ) and is invariant with range. The pulse length depends on the pulse duration,  $h = tc$ , where  $c$  is the speed of light and  $t$  is usually a few microseconds. The length of the pulse volume ( $h/2$ ), therefore, is approximately  $200$ – $300$  m for most radars. The location of the pulse volume in space is determined by the orientation of the antenna in azimuth and elevation and the slant range to the target. The slant range  $rs$  is determined by the time required for the pulse to travel to the target and be reflected back to the radar. The target is therefore uniquely defined in space by measurements of range, azimuth and elevation angle. A number of conical scans are performed according to the automatic scanning strategy of the radar antenna. The scanning strategy tries to form a constant altitude product at approximately a constant height above the ground (the lowest height is usually  $1.5$  km). Different scanning strategies are followed in each radar system (Shed *et al.* 1991). After the full volume of scans ( $5$ – $10$  min), a polar product is produced. The polar resolution in the horizontal plane is usually  $0.5$ – $1$  km in the radial direction. Further conversion from polar to Cartesian product is usually done using a nearest-neighborhood, or bi-linear, resampling method. In some other systems, the polar-to-Cartesian conversion is done while the data is acquired. Hence, the constant altitude radar grid may be considered to be referenced in a plane tangential to the Earth at the radar location as shown in Figure 3 (for more details, refer to Gad & Tsanis (2001)).

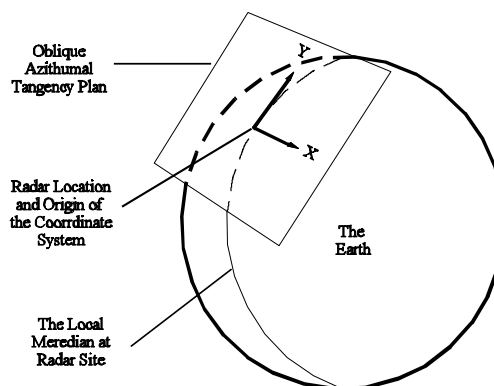


Figure 3 | Radar coordinate system with respect to the Earth.

### Format of the CAPPI product

After the full  $360^\circ$  scan of the radar, a CAPPI product is produced. The time separation between full scans, i.e. between files, is usually  $10$  min which constitutes the temporal resolution. The corresponding date and time of the data is normally included in the filenames. Note that date and time are in the UTC system.

There are two approaches that can be used for importing radar rainfall gridded data into GIS: (1) the coverage (vector) approach, and (2) the grid (raster) approach. In the coverage approach, the radar product would be treated as point coverage, in which each point is located at the centre of a rainfall cell. In the grid approach, the radar product is considered as raster data, i.e. a matrix of rows and columns. Treating radar data as raster data has one chief advantage over the vector approach because it requires considerably less computer resources in terms of storage, processing time and memory requirement. The reason is that, in the vector approach, a rainfall cell is represented by three variables ( $x$ ,  $y$  and rainfall value), whereas in the raster approach a rainfall cell is represented only by one variable (rainfall value). This is because the location of one rainfall cell from the whole grid is only required to reference the grid. This unique location is usually the lower left corner of the grid. In addition, GIS vector data require additional computer resources to handle their attributes. Because of the above reasons, the raster data approach was considered for this interface to manipulate radar data files.

```

Special Time String: #Numeric Definition File from King City Radar (WKR)
                    #Latitude: LonCentre 43.96350
                    #Longitude: LonCentre 79.57280
Product Information: #For Product: CAPPI
                    #At Valid Time: 200005100030
                    #Data Units: (MM/HR)
                    #Data Format: Binary
                    #Field Type Grid: Projection RadarProjection
                    #Scale 1.0:480:480:NearestNeighbour
Conversion Table:   TableLabels: PrecipitationRate-Reflectivity N DBZ MM/HR DBZ_SNOW CM/HR
                    TableStart: PrecipitationRate-Reflectivity
                    0 -999. -999. -999. -999. # 1 -31.5000 0.0004 -25.0000 0.0025;
                    2 -31.0000 0.0004 -24.5000 0.0026; 3 -30.5000 0.0005 -24.0000 0.0028;
                    4 -30.0000 0.0005 -23.5000 0.0029; 5 -29.5000 0.0005 -23.0000 0.0031;
                    6 -29.0000 0.0006 -22.5000 0.0032; 7 -28.5000 0.0006 -22.0000 0.0034;
                    :
                    :
Special Data String: #DATA-
                    :
Binary Data Section: :
                    :

```

Figure 4 | A typical header for radar data file.

Regarding the format and structure of the radar data file, the file contains a header part followed by a binary stream of one byte unsigned character values representing the records of the grid cells. Accordingly, the values range from 0–255 which is commonly referred to as the Iris  $N$  values, which is the reflectivity in  $\frac{1}{2}$ DBZ (DBZ is the radar reflectivity in decibels presented on a logarithmic scale), offset to  $-32$  DBZ. Such  $N$  values can be converted to reflectivity, rain rate or snow rate using a conversion table or using the corresponding equations. However, in some radar systems, the character values might represent the reflectivity values directly, i.e. 1 DBZ data resolution. Hence, one must refer to the data specifications for the variable represented by the one byte character value.

The header part is ASCII text containing information such as the radar name and location, date and time, and some other information. Figure 4 shows a typical header for a CAPPI data file. The valid time of the data file is written after a specific time string in the header, and the binary data section starts after another specific data string at the end of the header part. As shown in Figure 4, in our case, the time string is *At Valid Time:* and the data string is *#DATA*.

Two problems exist in the structure and format of the data and prevent ArcView GIS from loading the data properly. The first problem is that the data is in the form of binary character values. On the other hand, GIS does not support binary character values as external grid data sets. GIS supports two format for importing external grid data sets which are either space delimited ASCII values, or IEEE floating point binary values.

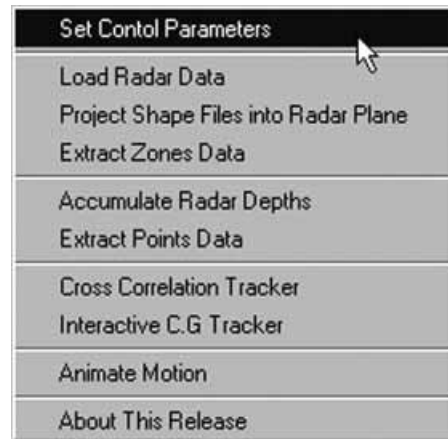
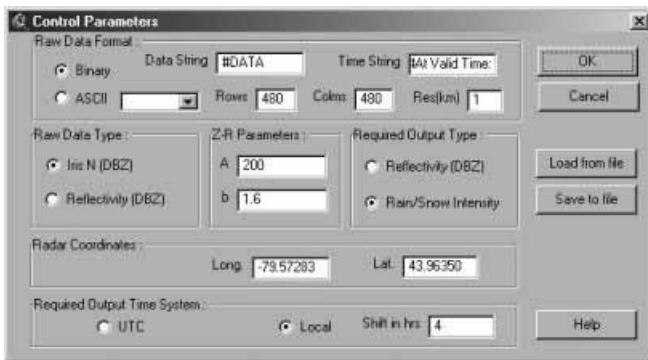


Figure 5 | The CAPPI menu (this menu is added to ArcView's graphical user interface after installation).

The second problem is that the data file obtained from some radar systems may proceed in an order incompatible with GIS. To explain the second problem, let us represent the radar image in 480 rows (each row consists of 480 cells), the problem is that the row at the bottom of the actual image is written at the beginning of the binary file in a standard right hand coordinate system. If the data is to be loaded into GIS as a grid data set, GIS assumes the first value in the file to be the upper left corner of the grid and proceeds to the bottom, i.e. GIS assumes the first row written in the data file to represent the top row in the grid data. Accordingly, if the data file is loaded in the original order into GIS, the result will be a reversed grid, which is totally different to the actual radar image.

## THE STRUCTURE OF THE GIS MODULE

After installation, the CAPPI menu is added to ArcView's graphical user interface, as shown in Figure 5. The CAPPI menu contains links to launch separate dialogs which interact with the user as well as interacting with the components of the interface. The first link in the menu launches the *Control Parameters* dialog which takes the user's input and holds parameters specifying the format and specifications of the data. These parameters must be specified by the user before any use is made of the



**Figure 6** | The control parameters dialog (this dialog holds data specifications as well as the required output format).

components of the module. Figure 6 shows a screen shot of the *Control Parameters* dialog. In addition to the description provided above, more information concerning these specifications parameters will be discussed in the following sections.

### Loading the data

A dynamic link library (*cappiload.dll*) and a calling script perform this task. The dynamic link library overcomes the two problems mentioned in the previous section. It has two procedures for loading radar data. One procedure handles binary data and the second is for ASCII data. The binary data procedure performs the following:

1. Reads the valid time from the header of the data file.
2. Scans the data file from the beginning to the string #DATA and forwards the file pointer to the beginning of the binary data section.
3. Reads the  $N$  binary character stream from the data file and converts the format into  $N$  IEEE binary floating point values.
4. Converts the  $N$  IEEE values into reflectivity, rain-rate, snow-rate, or keep the  $N$  values according to the user selection and input parameters specified in the specifications dialog.
5. Arrange the sequence of the data if necessary and write the output in a temporary binary IEEE floating point file.

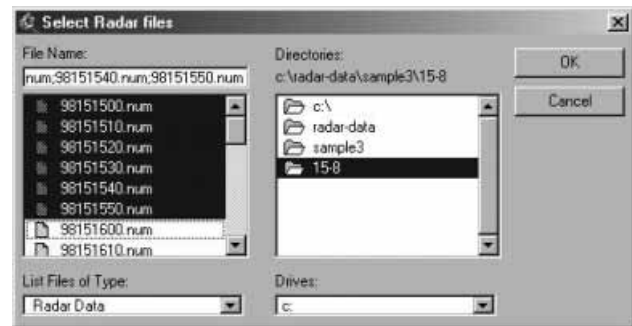


**Figure 7** | Screen shot of ArcView prompting for selecting radar data files to be loaded.

6. Return the valid time and an error checking handler.

A calling script is required to call this DLL and add the DLL's output as grids to ArcView. This calling script performs the following actions:

1. Ask the user to select the radar data files using a dialog.
2. Load the dynamic link library *cappiload.dll* and define the signatures of its internal procedures.
3. For each file of the user selected files, the script performs the following:
  - (i) Calls the loading procedure and passes it the path of the raw data file.
  - (ii) Loads the output of the loading procedure as a grid data set.
  - (iii) Loads the grid data set as a grid theme in the user specified view and renames it using the corresponding date and time obtained from the DLL's returns.
4. Drops the DLL.

The ASCII data procedure is similar to the binary procedure except that it accounts for reading different delimiters. The procedure used is determined from the data format and specifications which should be entered by the user in the specifications dialog. These control properties are required to be entered only once in an ArcView project, as the interface saves these properties with the project similarly to the built-in dialogs of ArcView properties. Figure 7 shows a screen shot of the interface prompting for user input to select data files for

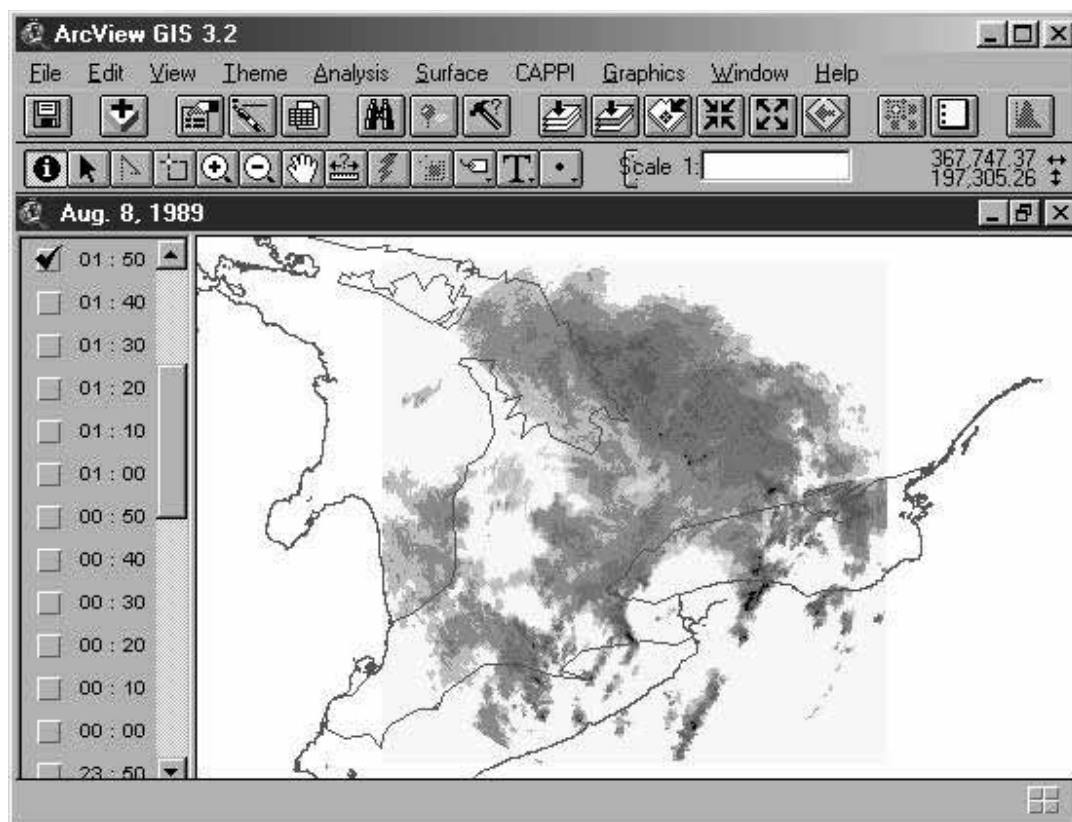


Figure 8 | Screen shot of ArcView after loading radar data files.

loading and Figure 8 is a screen shot of ArcView after loading the data.

### Coordinate system and projection

In order to properly reference the radar data with respect to other geographical features as well as the rain-gauge locations, both the geographical features and radar data must be referenced in the same projection and must use the same coordinate system. Radar CAPPI gridded data lies in an oblique plane tangential to the globe at the radar location (the origin) with its  $y$  axis parallel to the local geographic north at the radar location as shown in Figure 3. Geographical features as well as rain-gauges are usually in geodetic coordinates or in other projection systems. There are two solutions to this problem: (1) projecting the geographical features into the radar oblique

plane and performing the analysis in this plane, or (2) projecting both radar data and geographical features into another common projection system.

For applications which require data from a single radar (i.e. radar calibration using rain-gauges, small-scale severe weather warning or storm tracking for urban applications), the first solution is more convenient. This is because only one off-line projection operation is to be done to project geographical features into the radar coordinate system. Accordingly, radar data will be loaded as it is without projection, which saves time and computation. In addition, when the objective is the off-line calibration of radar using rain-gauges, the first solution is also more accurate because the projection of the radar grid alters the values of the rainfall cells due to the resampling effect. However, the resampling effect can be eliminated if the grid cells are treated as polygons, but this procedure is computationally demanding.

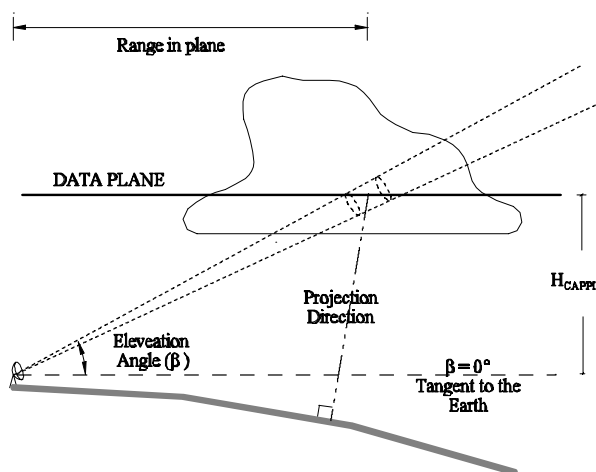


Figure 9 | A schematic diagram explaining the Gravitational Planner Projection method.

Because this interface focuses on single radar applications, the first solution was considered, i.e. performing the analysis in the radar plane. The remaining question now is the selection of the planar projection method that should be used to project geographical features and rain-gauges onto the radar plane. GIS software supports different oblique planner projections (for example, Sterographic, Gnomonic, Equidistant and Lambert). All the above-mentioned oblique planar projections are supported only on a sphere (ArcDoc 7, 1994). On the other hand, coordinates of the geographical features or rain-gauge are generally geodetically based. The GIS methodology followed when converting from ellipsoid-based projections into sphere-based projections is done by interpreting the geodetic coordinates as geocentric ones. For points having maximum east/west distance from the radar, such a methodology can introduce a maximum error of approximately 1 km in locating these points if their geodetic coordinates are interpreted as geocentric ones (Gad & Tsanis 2001). A new ellipsoid-based projection method (the GPP: Gravitational Planner Projection) was developed for the accurate positioning of rain-gauges as well as other geographical features into the radar plane or vice versa. This method is based on the gravity direction, which is the normal to the reference ellipsoid at the point being projected, as shown in Figure 9. The details and equations

of the GPP projection method can be found in Gad & Tsanis (2001).

The dynamically linked library (*cappiproj.dll*) is responsible for projecting the user-selected shapefiles into the radar plane. This library is independent of ArcView classes, i.e. it has its own read/write routines for handling shapefiles. Details of the shapefile format can be found in an ESRI white paper (1998). Hence, this library is a standalone application which can be linked to any other software which supports a shapefiles binary format. The GPP inverse transformation is included within the procedures of this library. In addition, the sphere-based azimuthal equidistant projection (using pre-conversion from geodetic to geocentric coordinates) is available also in the library. The functions of *cappiproj.dll* can be summarized in the following steps:

1. Open the original shapefile \*.shp and index file \*.shx for binary read access.
2. Identify shape type (i.e. point, line or polygon).
3. Create the new \*.shp and \*.shx files for output in binary write mode.
4. For each shape in the input shapefile:
  - (i) Read the shape into a corresponding temporary shape object.
  - (ii) Obtain shape vertices.
  - (iii) Call the projection routine to project all vertices.
  - (iv) Update vertices and bounding box of the shape object
  - (v) Write the updated shape information into the output shapefile.
  - (vi) Update the header of the shapefile.
  - (vii) Delete the shape object.
5. Copy the input DBF file as an output DBF file and rename it to be consistent with the output \*.shp and \*.shx file names.
6. Close input/output shape and index files.

A calling script is required to call this library. In addition to the interaction with *cappiproj.dll*, the calling script prompts for the required name and path of the output shapefile and whether or not to add the projected shapefile to the view which represents the radar CAPPI data plane.

## ACCUMULATING RADAR RAINFALL DEPTHS

When the user selects to load and convert radar data to rainfall rate, the  $Z$ - $R$  parameters must be specified in the dialog described above. The application of a  $Z$ - $R$  relation produces instantaneous rainfall intensity maps. In order to develop maps of rainfall accumulations, a method for calculating rainfall depths is essential. The simplest method is the one employing the assumption of stationary rainfall intensity in space and time (during the sampling interval). However, the precipitation field moves at an approximately constant speed and direction during the sampling interval. In addition, rainfall intensity changes during the sampling interval. The interface component responsible for accumulating rainfall depths implements three methods for calculating rainfall accumulations: (1) assuming no advection, i.e. no velocity vector, (2) taking the velocity vector into account and neglecting the effect of the growth/decay, and (3) taking the effects of both the velocity vector and the growth/decay of rainfall by assuming linear variation in the rainfall intensity. A brief description of these three methods follows.

### Method 1

In this method, the rainfall field is assumed to remain stationary in space during the sampling interval (10 min). Accordingly, rainfall depths during each sampling interval are simply calculated by multiplying the rainfall rates by the sampling interval (10 min). Finally, the accumulation map during a certain accumulation period, or *output interval* (1 h, for example), is obtained by adding the contributions from all sampling intervals included in the accumulation period.

### Method 2

The rainfall field is assumed to move and spread into accumulations according to the velocity vector, i.e. the rainfall field is not assumed to be stationary in space during the sampling interval. To account for this, the sampling interval (10 min) is divided into smaller *sub-intervals* of duration called the *analysis step* (1 min, for

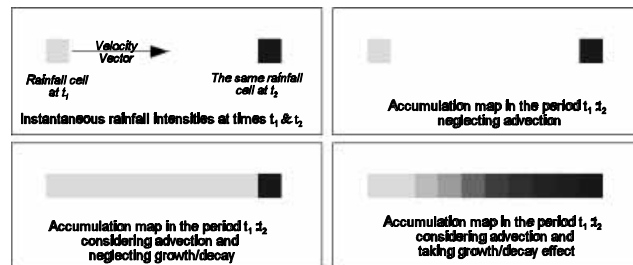


Figure 10 | A schematic diagram representing the three different methods used for accumulating rainfall depths.

example). At each sub-interval, the original radar rainfall field is shifted according to the advection velocity vector and placed in the resulting grid cells. The accumulations during the sampling interval are the sum of the accumulations of the original field during one analysis step as well as all other accumulations during the intermediate sub-intervals. Finally, the accumulation map during a certain accumulation period (1 h, for example) is obtained by adding the contributions from all sampling interval maps, or in other words, the accumulations during all analysis steps or sub-intervals within the *output interval*.

### Method 3

The theory of this method is similar to that of method 2 except that it allows the advected rainfall field to vary linearly in order to reach the final rainfall field at the end of the sampling interval. This is done by weighting (according to the time offset) a copy of the original rainfall field at the beginning of the sampling interval before shifting it to the proposed location.

Figure 10 shows a schematic diagram explaining the three accumulation methods. More details and applications of the above three methods can be found in Bellon & Austin (1984), Austin (1987), Blanchet *et al.* (1991), Brown *et al.* (1991) and Fabry *et al.* (1994). The following inputs are essential to run the interface component: (1) starting and ending times, (2) the output interval for calculating radar depths, i.e. time separation between output grids, and (3) selecting a method for accumulating the radar rainfall depths.

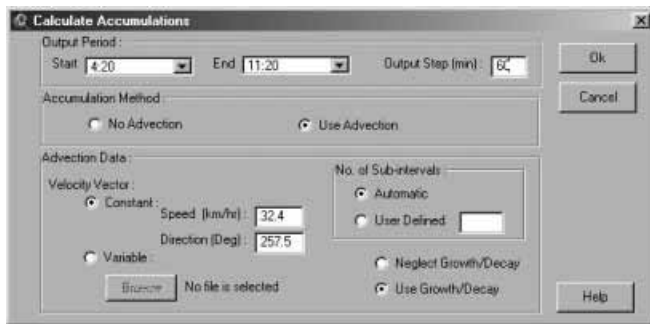


**Figure 11** | The accumulations dialogue prompting for user input to calculate rainfall depths.

Methods (2) and (3), described above, require additional user input to specify the speed and direction of rainfall patterns as well as the number of sub-intervals. The kinematic characteristics (speed and direction) of rainfall can be obtained using the kinematic component described later. Figure 11 shows a screen shot of the accumulation dialog prompting for user input for calculating radar rainfall depths. The output of this component of the interface is in the form of a series of GIS grids representing rainfall depths at every output step in the selected period. The new grids are placed in a new view which is uniquely named by the time parameters (starting time, ending times and output interval). Figure 12 shows a sample output using the three different accumulation methods.

It is important to highlight some points on the selection of the *analysis step* or, in other words, the number of *sub-intervals*. It might be thought that a smaller analysis step may increase the accuracy of the calculated accumulations. However, this rule is only valid to a certain limit, below which no significant improvements in the accuracy of the estimates can be achieved. In addition, a very small analysis step can increase the run time significantly. Accordingly, it is important to select the analysis step properly. The selection of the analysis step should be consistent with both the spatial resolution of the radar grid and the velocity vector. For example, for fast moving rainfall fields, a smaller analysis step must be chosen in order to capture the moving rainfall field at all grid cells. On the other hand, a small analysis step for a slow moving

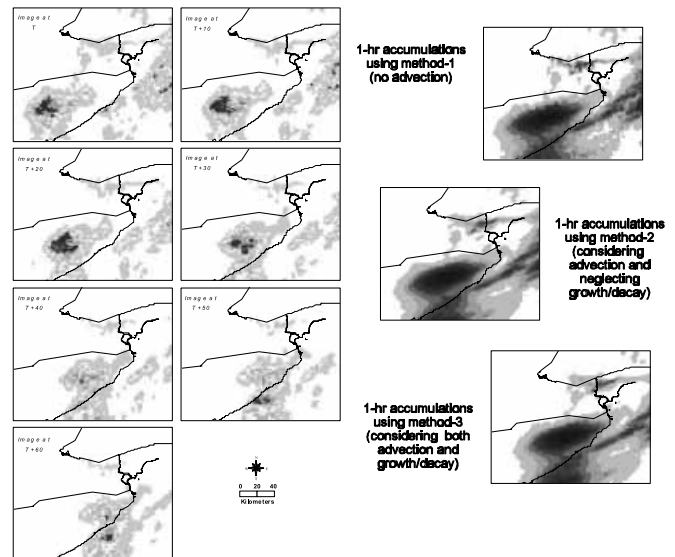


**Figure 12** | A sample case of accumulating 1 h depths. The seven images on the left are instantaneous rainfall intensity maps covering 1 h, whereas the three maps on the right are accumulation maps produced using the three different accumulation methods.

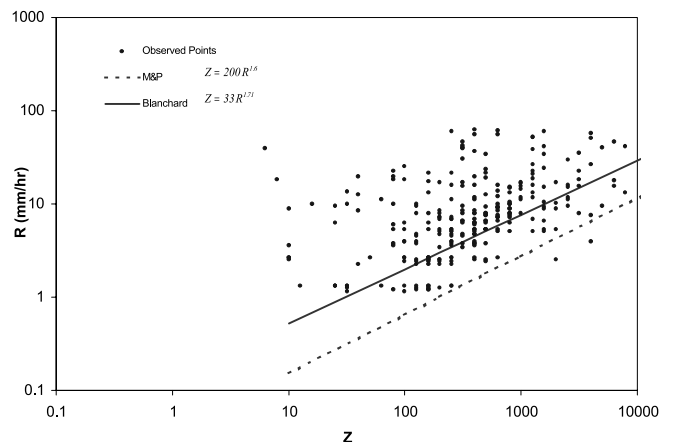


**Figure 13** | Radar reflectivity versus rain gauge estimated rainfall rate.

rainfall field is unnecessary because it will increase run time without improving the accuracy that would be obtained using a larger analysis step. As shown in Figure 11, the user can choose to enter the value of the number of sub-intervals or leave this to be done automatically by the interface. The interface determines automatically the analysis step and the corresponding number of sub-intervals by calculating the time required by the velocity vector to travel a distance equal to the grid

resolution. Then this travel time is approximated to satisfy an integer number of sub-intervals.

It should be noted that special care should be taken when interpreting the accumulations calculated using methods (2) or (3) at the edges of the radar domain (the edges from which the velocity vector advances). The reason for this is that zero values are advected at this edge as no radar data exists beyond the edges. Accordingly, there is an uncertainty associated with the accumulations in a strip of width equal to the velocity multiplied by the sampling interval at the edge of the radar domain from which the rainfall pattern advances.

### COMPARISON WITH RAIN-GAUGE DATA

Radar rainfall accumulations are usually compared to rain-gauge depths. Different factors affect such comparisons. One of the main factors affecting this comparison arises due to errors in the radar measurements. Applying the black box concept which involves the calibration of the  $Z-R$  relation using accurate rain-gauge measurements reduces the effect of these errors. However, there are other factors affecting this comparison, such as: (1) the processes taking place between the radar measurements height and the ground, such as evaporation and wind drift (Collier 1999), (2) errors in the rain-gauge measurements (Habib *et al.* 2001), (3) the difference between point measurements and areal averages, and (4) the advection correction method used in accumulating the radar depths. Some of the previously mentioned errors may be referred to as *sampling errors* (Kitchen & Blackall 1992). Previous and current research focuses on reducing the bias and fluctuations in radar sensation of precipitation. Accordingly, a user-friendly, flexible and accurate interface for performing such analysis can facilitate such studies and provide a valuable tool for researchers working in this field. The GIS interface component responsible for this analysis performs the typical GIS intersection operation of the point (rain-gauge) locations on the user-selected radar rainfall grids and outputs the corresponding radar accumulations in an output text file. This component of the interface requires the following input from the user: (a) point theme representing rain-gauge locations, (b) the

starting and ending times, and (c) name and path of the output text file.

The interface is currently employed to compare rainfall accumulations calculated using the three accumulation methods to the corresponding rain-gauge accumulations and using different accumulation intervals. However, Figure 13 shows a comparison of rain-gauge rainfall rate averaged on a 10-minute interval and radar reflectivity method (1) (no advection) for four convective storm events in the summer of 1989. As shown in the figure, there is some evidence of underestimating rainfall rates using the classical MP  $Z-R$  relation (Marshall & Palmer 1948) using method (1) (no advection). However, more data is required to achieve a general conclusion. Details of the tipping bucket rain-gauge network used to produce Figure 13, as well as the computer utilities required for pre-processing tipping bucket rain-gauge data, can be found in Tsanis & Gad (2001).

### RAINFALL KINEMATICS

One method to study the storm motion is by tracking the centre of gravity of the rain area (Wilk & Gray 1970; Barclay & Wilk 1970; Zittel 1976; Bellon & Austin 1976; Bjerkaas & Forsyth 1980; and others). If echoes can be delineated easily, then this procedure might be the simplest effective pattern-matching procedure. In the automatic operation of this technique, constraints are usually imposed to aid the matching procedure, such as the minimum and maximum speed used to establish a search region for the next storm centroid to be marked as the same storm. However, problems usually arise because of the variable nature of rainfall (growth and decay) which affects the location of the centre of gravity that may lead to ambiguities in the estimated storm characteristics. Other problems appear in cases of widespread rainfall patterns which produce difficulties in isolating storm clusters.

Another method of estimating the kinematics of rainfall is by cross-correlating a portion or the whole radar domain with subsequent scans. This procedure has the advantage of taking into account the detailed shape of the echo being tracked, and decreases the chances of mismatching echoes (Wilson 1966; Zawadzki 1973; Austin

**Table 1** | Performance of the different components of the GIS module

Operation	Average run time (s)	Written using
Loading one radar file (480 × 480 array) in ArcView		
Binary	< 0.5	C + + and Avenue
ASCII	0.5–1	C + + and Avenue
Projecting a polygon shapefile (1000 records, 20 vertices per polygon in average)		
	2–3	C + + and Avenue
Accumulating radar depths in one sampling interval		
Method (1): no advection	1–2	Avenue
Method (2): advection (no G/D) using 10 sub-intervals	9–13	Avenue
Method (3): advection (taking G/D) using 10 sub-intervals	10–15	Avenue
Extracting radar data for one image at locations of 100 points		
	1–2	Avenue
Storm kinematics using the whole radar domain for an intermediate sampling interval		
Centroid module	4–6	Avenue
Cross-correlation module		
Search option 1	500–600	Avenue
Search option 2	120–150	Avenue
Search option 3	10–20	Avenue
Extracting portion of one radar image in a data file		
IEEE floating point binary format	1–2	Avenue
ASCII space delimited format	2–3	Avenue

& Bellon 1974; Hill *et al.* 1977; Yoshino & Kozeki 1985; Collier 1989; Li *et al.* 1995; and others). If the echoes in the radar image move together and there are no significant intensity or shape changes, this technique can be considered the most accurate and simplest matching technique. However, other methods exist for matching echoes at separate times in order to estimate echo displacement vectors, such as minimising the error sum of squares (Duda & Blackmer 1972).

The GIS module implements two methods for estimating rainfall kinematics: (1) the echo centroid technique and (2) the cross-correlation technique.

### Echo centroid method

Because this release of the interface concentrates mainly on offline applications of weather radar data, it was

decided to design this module to work in an interactive mode. The task of delineating separate storm areas is left to the user. This is done using the pointing device. The user performs the following tasks to complete a tracking session: (1) starts a new session, (2) activates a rainfall grid as the current grid, (3) delineates the echo of interest, (4) repeats steps (2) and (3) for all time steps required and finishes the session to display the results of the tracking session, and (5) saves the tracking session in a text file.

A threshold can be applied to identify particular intensity zones. This module was written using avenue scripts which perform the following interactive actions:

1. Obtain the polygon drawn by the user.
2. Use the obtained polygon to clip the portion under interest from the whole radar domain.
3. Assign zero values to areas below the threshold value, performs a 2D centre of mass for the clipped zone, and adds the  $x$  and  $y$  coordinates of the centroid to a global list.
4. Once the user clicks the finish button, the module calculates the velocity vector from the positions of each two consecutive centroids in the global list and displays the average velocity vector as well as its standard deviation.
5. Upon clicking the *save session* button, the module saves a text file containing all details of the session including the coordinates of the centroid at the different times, the velocity vector at each time, and the final average and standard deviation of the velocity vector.

### Cross-correlation method

This module was written using avenue scripts and allows correlating selected portions of the whole domain with the corresponding subsequent scan. It works by shifting the current clipped rainfall gridded data by a variety of grid lengths and finding the optimum spatial shift corresponding to maximum correlation with the grid at the previous time. A threshold value may also be used under which the grid cells are marked with zeros. The results of this tracker

are reported as the optimum spatial shift ( $dx_{opt}$ ,  $dy_{opt}$ ) in  $x$  and  $y$  directions, respectively, as well as the corresponding velocity vector that maximises the correlation coefficient between the shifted copy of the current rainfall grid and the previous rainfall grid. The mean motion of the precipitation field, i.e. the velocity vector in km/h, is given by  $(-dx_{opt}/_t, -dy_{opt}/_t)$  where  $dx_{opt}$  and  $dy_{opt}$  are in kilometres and  $_t$  is the time separation in h. This module runs automatically, i.e. the user can select radar rainfall grids at different times and the module moves from one image to the next until it finishes all rainfall grids within the selected time period. Three options are available for performing the search for an optimum spatial shift:

1. The first option is by trying all possible shifts in  $x$  and  $y$  which are within the constraints (min and max speed entered in the dialog).
2. The second option is faster than the first one. It performs the full search at the beginning, then it allows the module to focus the search at the following time in a  $90^\circ$  quadrant around the direction obtained in the previous step.
3. The third option is the fastest search method which employs the principle of response surface analysis to perform the search only on the directions of maximum slope of the correlation surface, i.e. by climbing the short route on the correlation surface to the global maxima. In a few cases, the search may result in a local maxima instead of a global maxima.

### TECHNICAL DETAILS

An animation component is provided in the module. This animation module has the advantage of animating storm motion in more than one view at the same time, hence allowing zooming to different scales. This provides a good tool, especially when monitoring storm evolution at different scales at the same time. In addition, the animation module allows zooming inside the same view while the animation is running. Another component is available for the purpose of re-delivering radar data. The aim of this component is to reproduce sets of radar data files clipped in a certain portion under the radar umbrella.

## Installation

The module is available in a set-up file. The installation effect is summarized in the following: (1) all dynamic link libraries are extracted to \$AVHOME\AV\_GIS30\ARCVIEW\BIN32\, (2) the extension file cappi.avx is extracted to \$AVHOME\AV\_GIS30\ARCVIEW\EXT32\ (3) the directory \$AVHOME\AV\_GIS30\ARCVIEW\CAPPI\ is created and the executable files, legend files, documentation files, as well as the uninstall program, are extracted inside this directory, where \$AVHOME denotes the ArcView installation directory. It should be noted that some of the dynamic link libraries used in this interface are also provided in separate executable versions in the installation package for separate usage from the DOS prompt.

## Performance

The module handles different operations such as loading and writing data, projecting geographical features into the radar plane, accumulating rainfall depths, comparison with rain-gauge data, animating storm evolution on top of other geographical features, and estimating storm kinematics. In addition to the interface components developed in this study, we believe that the main advantage exists in bringing radar data to the GIS environment in which different useful analysis requests are available.

In order to fully summarise the performance of the different components of the module, the run time for some operations on a PIII 600 MHz (256 MB RAM) PC is shown in Table 1.

Most of the operations performed by the module may be considered to have acceptable run times except for a few operations such as estimating rainfall kinematics using the cross-correlation technique (options 1 and 2). Improvements are currently investigated to reduce the run time by substituting some of the avenue requests involved by external procedures (dynamic link libraries). The reason for this is that some grid requests in ArcView cause the grids to be written to the computer hard drive. Hence if these disk write/read operations are avoided, the run time is expected to decrease relatively. However, the use

of search option 3 decreases run time significantly but it should be noted again that it cannot be trusted in all cases in the current release of this module.

Future releases of this interface will aim to include the following upgrades: (1) run time improvements for the cross-correlation tracker (options 1 and 2) as well as a more objective and stable strategy for option 3, (2) removal of ground clutter from the data, and (3) a real-time mode for forecasting purposes.

## ACKNOWLEDGEMENTS

The authors would like to thank the City of Hamilton for providing the rainfall data from their Rainfall Monitoring Network and the King City Weather Radar Station for providing the radar data. The present work was supported by the City of Hamilton via a collaborative agreement and by the National Science and Engineering Research Council research grant No. OGP0157914.

## REFERENCES

- Amorocho, J. & Wu, B. 1977 Mathematical models for simulation of cyclonic storm sequences and precipitation fields. *J. Hydrol.* **32**, 329–345.
- ArcDoc Version 7.0 1994 Environmental Systems Research Institute (ESRI), Redlands, CA.
- Atlas, D. 1964 *Advances in Radar Meteorology. Advances in Geophysics*, vol. 10 (ed. H. E. Landsberg & J. Van Meighen) Academic Press, New York.
- Atlas, D. (ed.) 1990 *Radar in Meteorology: Battan Memorial and 40th Anniversary Radar Meteorology Conference*. American Meteorological Society, Boston, MA.
- Austin, G. L. & Bellon, A. 1974 The use of digital weather record for short-term precipitation forecasting. *Q. J. R. Meteorol. Soc.* **100**, 658–664.
- Austin, P. M. 1987 Relation between measured radar reflectivity and surface rainfall. *Mon. Weather Rev.* **115**, 1053–1070.
- Austin, P. M. & Houze R. A. 1972 Analysis of the structure of precipitation patterns in New England. *J. Appl. Meteorol.* **11**, 926–934.
- Barclay, P. A. & Wilk, K. E. 1970 *Severe Thunderstorm Radar Echo Motion and Related Weather Events Hazardous to Aviation Operations*. ESSA Technical Memorandum No. ERLTM-NSSL 46.

- Battan, L. J. 1981 *Radar Observation of the Atmosphere*. University of Chicago Press, Chicago.
- Bellon, A. & Austin, G. 1976 The real-time test and evaluation of SHARP. A short term precipitation forecasting procedure. *17th Conf. on Radar Meteorology, American Meteorological Society, Atlanta, GA*. American Meteorological Society, 522–525.
- Bellon, A. & Austin, G. L. 1984 The accuracy of short-term radar rainfall forecasts. *J. Hydrol.* **70**, 35–49.
- Bjerkaas, C. L. & Forsyth, D. E. 1980 *An Automated Real-Time Storm Analysis and Storm Tracking Program (WEATRK)*. AFGL-TR-80-0316, Air Force Geophysics Laboratory.
- Blanchet, B., Neuman, A., Jacquet, G. & Andrieu, H. 1991 Improvement of rainfall measurements due to accurate synchronization of rain gauges and due to advection use in calibration. In: *Hydrological Application of Weather Radar* (ed. I. D. Cluckie & C. G. Collier), pp. 213–218. Ellis Horwood, Chichester
- Brown, R., Sargent, G. P., Newcomp, P. D., Cheung-Lee, J. & Brown, P. M. 1991 Development of the FRONTIERS precipitation nowcasting system to use mesoscale model products. *25th Conf. on Radar Meteorology, 24–28 June, 1991, Paris, France*. American Meteorological Society, Boston, MA, pp. 79–82. Preprints.
- Collier, C. G. 1989 *Application of Weather Radar Systems: A Guide to Use of Radar Data in Meteorology and Hydrology*. Ellis Horwood, Chichester.
- Collier, C. G. 1999 The impact of wind drift on the utility of very high spatial resolution radar data over urban areas. *Phys. Chem. Earth (B)* **24**, 889–893.
- Doviak, R. J. & Zrnic, D. S. 1993 *Doppler Radar and Weather Observations*, 2nd edn. Academic Press, San Diego.
- Duda, R. O. & Blackmer, R. H. 1972 *Application of Pattern Recognition Techniques to Digitised Weather Radar*. Report (Contract No. 1-36072). SRI project No. 1287. Stanford Research Institute, Menlo Park, CA.
- ESRI 1998 ESRI Shapefile Technical Description. An ESRI White Paper. July. Environmental Systems Research Institute (ESRI), Redlands, CA.
- Fabry, F., Bellon, A., Duncan, M. R. & Austin, G. L. 1994 High resolution rainfall measurements by radar for very small basins: the sampling problem reexamined. *J. Hydrol.* **161**, 415–428.
- Gad, M. A. & Tsanis, I. K. In press The ellipsoid-based gravitational planner projection – GPP. *J. Hydrol. Engng ASCE*.
- Gupta, V. K. & Waymyre, E.C. 1979 A stochastic kinematic study of subsynoptic space-time rainfall. *Wat. Res. Res.* **3**(15), 637–644.
- Habib, E., Krajewski, W. F. & Kruger, A. 2001 Sampling errors of tipping-bucket rain gauge measurements. *J. Hydrol. Engng.* **6**(2), 159–166.
- Hill, F. F., Whyte, K. W. & Browing, K. A. 1977 The contribution of a weather radar network for forecasting frontal precipitation; a case study. *Meteorol. Mag.* **106**, 68–89.
- Huff, F. A., Vogel, J. L. & Changnon, S. A. Jr. 1981 Real-time rainfall monitoring – prediction system and urban hydrologic operations. *ASCE J. Wat. Res. Plan. Mngnt.* **107**(WR2), 419–435.
- Joe, P. 1999 *Precipitation at the Ground: Radar Techniques*. Internal Document. Atmospheric Environment Service of Canada, Meteorological Research Branch, Cloud Physics Research Division, 4905 Dufferin St., Downsview, Ontario, Canada M3H 5T4.
- Kitchen, M. & Blackall, R. M. 1992 Representative errors in comparisons between radar and rain-gauge measurements of rainfall. *J. Hydrol.* **234**, 13–33.
- Li, L., Schmid, W. & Joss, J. 1995 nowcasting of motion and growth of precipitation with radar over a complex orography. *J. Appl. Meteorol.* **34**, 1286–1300.
- Marshal, J. S. & Palmer, W. 1948 The distribution of raindrops with size. *J. Meteorol.* **5**, 165–166.
- Rinehart, R. E. 1991 *Radar for Meteorologists*. University of North Dakota, Grand Forks, ND.
- Sauvageot, H. 1982 *Radarmeteorologie*. Eyrolles, Paris.
- Skolnik, M. (ed.) 1970 *Radar Handbook*. McGraw-Hill, New York.
- Tsanis, I. K. & Gad, M. A. 2001 A GIS precipitation method for analysis of storm kinematics. *J. Environ. Model. Software.* **16**, 273–281.
- Wilk, K. E. & Gray, K. C. 1970 Processing and analysis techniques used with the NSSL weather radar system. *14th Conf. on Radar Meteorology*. American Meteorological Society, Boston, MA, pp. 369–374 (preprint volume).
- Wilson, J. W. 1966 *Movement and Predictability of Radar Echoes*. Report, US Weather Bureau Contract CWB-11093, The Travelers Weather Research Center, Hartford, CT.
- Yoshino F. & Kozeki, D. 1985 *Study on Short-Term Forecasting of rainfall using Radar Rain-gauge*. Report, Hydrology Division, Public Works Research Institute, Ministry of Construction, Japan.
- Zawadzki, I. I. 1973 Statistical properties of precipitation patterns. *J. Appl. Meteorol.* **12**, 459–472.
- Zittel, W. D. 1976 Computer applications and techniques for storm tracking and warning. *17th Conf. on Radar Meteorology, Seattle, WA*. American Meteorological Society, Boston, MA, pp. 514–521 (preprint volume)